Z. Kristallogr. **221** (2006) 621–634 / **DOI** 10.1524/zkri.2006.221.9.621

Deformed model sets and distorted Penrose tilings

Bernd Sing*,[I] and T. Richard Welberry[II]

[I] Fakultät für Mathematik, Universität Bielefeld, Universitätsstraße 25, 33615 Bielefeld, Germany
[II] Research School of Chemistry, Australian National University, Canberra, ACT 0200, Australia

Received November 2, 2005; accepted February 18, 2006

Quasicrystals / Deformed model sets / Size effect / Penrose tiling / Monte-Carlo simulation

Abstract. In this article, we show how the mathematical concept of a deformed model set can be used to gain insight into the diffraction pattern of quasicrystalline structures. We explain what a deformed model set is, what its characteristic features are and how it relates to certain disorder phenomena in solids. We then apply this concept to distorted Penrose tilings, *i.e.*, Penrose tilings where we apply size-effect-like distortions. While the size effect in crystals only operates on the diffuse scattering, there is also an intensity transfer on the Bragg peaks in distorted Penrose tilings. The persistence of pure point diffraction in distorted Penrose tilings can be explained by interpreting such tilings as deformed model sets.

1. Introduction

Ever since their first discovery in 1984 [32, 22], quasicrystals (materials displaying symmetries forbidden in classical crystallography) have been the subject of intense study by both experimental and theoretical scientists. During most of this time extensive use has been made of tiling models such as the Penrose tiling to aid the understanding of the exact nature of their structure. The Penrose tiling provides an attractively simple extension of conventional crystallography in that the conventional single "unit cell" is now replaced by two different "tiles" (*e.g.*, a fat and a thin rhombus in 2D), each of which can be decorated by an arrangement of atoms. The so-called "matching rules", which define the way in which tiles can be assembled to form the Penrose pattern, ensure that the same local structure is preserved across tile boundaries. However, real quasicrystals do not conform to this simple Penrose tiling picture, although the analogy is sufficiently close (at least on average) that such tiling patterns are often superimposed on structural models to aid interpretation. In saying that quasicrystals do not conform to this simple two-tile picture we mean that, while such a model will give sharp Bragg reflections at points corresponding to the observed quasicrystal diffraction pattern, it does not seem possible to decorate the tiles in a way which will reproduce the observed Bragg peak intensities [34].

The tiling analogy has nevertheless remained useful and has been used to explore other aspects of quasicrystallinity. In a previous paper [41] the possibility was explored, using the Penrose tiling pattern, that local distortions can occur in quasicrystals similar to those that result from the atomic size-effect in conventional crystalline alloys. This work was prompted by the observation of the diffraction pattern of the decagonal quasicrystal $Al_{71}Co_{13}Ni_{16}$ [15]. In the zero-level ($h_5 = 0$) section[1] of the diffraction pattern of this system there is a clearly delineated decagon. On the inside of this decagon, there is generally low intensity, while on the outside the intensity is markedly higher. These features closely resemble ones that are observed in disordered *crystalline* materials, which are attributable to the so-called "atomic size-effect". The "size-effect" was first shown to occur in metal alloys [35], but has subsequently been found in many quite different disordered crystalline systems (*e.g.*, cubic zirconia (CSZ) [38], wüstite [39], urea inclusion compounds [42], $KLiSO_4$ [40]).

The size-effect in *crystalline* materials occurs when there is a coupling of the displacement of a site with its occupancy. It may be most easily understood in terms of the simple example of a disordered binary alloy in which lattice sites are occupied by two different atomic species with different atomic radii. Although nominally the atoms are all assumed to reside on the sites of the average lattice, relaxation takes place locally. Neighbouring atoms tend to move apart if they are both large, or closer together if they are both small. Such local shifts are transmitted to more distant neighbours and the relaxation spreads throughout the lattice to minimise the overall strain. This simple effect produces a very characteristic feature in the diffraction pattern. The intensity of diffuse

* Correspondence author (e-mail: sing@math.uni-bielefeld.de)

[1] Decagonal quasicrystals are axial quasicrystals, *i.e.*, they are quasiperiodic in two dimensions and periodic in the third one. To index the Bragg peaks in such a structure, one needs five indices: Four because of the quasiperiodicity in two dimensions $(h_1, \ldots, h_4)$ and one (h_5) for the periodic direction, see [34].

scattering is diminished on one side of a plane that passes through Bragg positions and is enhanced on the other. The plane involved occurs at a distance (from the origin) which is reciprocal to the mean inter-atomic vector along which the local inter-atomic interactions take place.

In the previous paper [41], Monte Carlo simulation was used to induce size-effect-like distortions in a perfect Penrose tiling pattern by applying forces which attempted to stretch the bonds (*i.e.*, the edges of the rhombi) between some kinds of vertices of the tiling and to contract others. The resulting diffraction pattern, calculated with a simple decoration of the tiling in which a single atom was placed at each vertex, convincingly showed a similar kind of "intensity transfer" to that which is characteristic of size-effect distortions in crystals. One major difference was that here the distorted tiling patterns did not produce substantial amounts of diffuse scattering and the changes in intensity were mainly in the Bragg peaks themselves. [It should be noted that because of the inherent randomness in the Monte Carlo simulation some diffuse scattering was inevitably present.] The distorted tiling pattern was still topologically identical to the original Penrose tiling (*i.e.*, it had the same connectedness, so both tilings are isomorphic as (infinite) graphs), and the simulated patterns still had a quasicrystalline diffraction pattern and Bragg peaks occurred in the same positions, but with drastically different intensities. This is quite different from the crystalline case, where local changes in the shapes and sizes of "unit cells" affect the intensity of the Bragg peaks only via the slowly-varying Debye-Waller factor. On the other hand, they strongly affect the diffuse scattering that originates from occupancy disorder.

It thus emerges from the above discussion that the Bragg intensities of a quasicrystalline diffraction pattern may not only be affected by the details of the atomic decorations but also by the kinds of local distortion that might be present. It is therefore important to assess whether this way of looking at a quasicrystalline structure is of general use in structure determination and in understanding quasicrystals generally. One of the aims of the present work is to try to put the results of the previous study [41] on a more rigorous mathematical footing. The particular focus of the present paper resulted from the observation that the example distorted Penrose patterns produced in [41] by Monte Carlo simulation appeared to be closely related to certain so-called *deformed model sets* that have recently been of interest to theoreticians [12, 3]. Consequently, in Section 2 of this article, we review the mathematics to describe such deformed model sets and discuss their relationship to the crystalline concepts described above. Then in Section 3 we give, in the light of this formalism, a detailed discussion of the particular distorted Penrose tilings described earlier.

2. Deformed model sets

2.1 Cut-and-project schemes

One of the most striking features (which also led to their discovery [32, 22]) of (idealised) quasicrystals is their diffraction pattern: They are pure point diffractive[2], *i.e.*, show Bragg peaks only (and therefore have some sort of long-range order), but their diffraction patterns show extraordinary symmetries like fivefold axes (which are impossible for periodic crystals in 3-dimensional space). This raised the question how such structures, which cannot be periodic, can be described appropriately; here, the description in terms of some kind of projection method was most successful [24]. The justification for this method, however, became clear only recently. This is described (mathematically rigorous) in [6] (also see the review articles [8, 7]).

We give here a brief outline of the important concepts. Let us assume the following properties:

- **A1** The atoms of the structure are well separated (which implies the mathematical statement that the measure which models the structure is translation bounded [6, Axiom 1]).
- **A2** The (volume averaged) autocorrelation coefficients $\eta(z)$ at Position z exist [6, Axiom 2].
- **A3** Points in the set $\{z \mid \eta(z) \neq 0\}$ are not arbitrarily close [6, Axiom 3^+], *i.e.*, (relevant) inter-atomic distances are not too similar.
- **A4** The structure in question is pure point diffractive.

The first two properties are automatically fulfilled for (real) physical systems, whereas the latter two indicate that some kind of order is present (and not an amorphous material). In the context of **A1**, we also introduce the notion of a *Delone set* (or *Delaunay set*): A set $S \subset \mathbb{R}^d$ is a Delone set iff it is uniformly discrete and relatively dense. Here, *uniformly discrete* means that there is a number $r > 0$ such that each (open) ball of radius r contains at most one point of S. The maximal such r is the packing radius for S. On the other hand, S is *relatively dense* if there is a number $R > 0$ such that each (closed) ball of radius R contains at least one point of S. The minimal such R is the covering radius of S. (Bulk) Solids (even amorphous) are Delone sets, and Delone sets fulfill **A1**.

For a given structure, the four properties **A1–A4** already determine an essentially unique (*i.e.*, unique up to isomorphism) *cut-and-project scheme* $(\mathbb{R}^d, H, \tilde{L})$: The *physical* or *direct space* is given by $\mathbb{R}^d$, the d-dimensional Euclidean space (usually, we have $d = 2$ or 3), sometimes also denoted by $\mathbb{E}^d$. We denote the *internal space* by H, which is often also given by a Euclidean space $H = \mathbb{R}^m$ (for some m), but also some more exotic spaces are possible (see the above articles and references therein). In the product space $\mathbb{R}^d \times H$, a lattice $\tilde{L}$ is given such that the (canonical) projection π of it into the direct space is one-to-one (so $\pi : \tilde{L} \to L = \pi(\tilde{L})$ is a bijection[3]) and the (canonical) projection π_{int} into the internal space has dense image ($L^* = \pi_{\text{int}}(\tilde{L})$ is dense in H). This situation is schematically summarised as follows (as usual, we denote by

[2] Of course, real-world quasicrystals do have diffuse scattering, but in this section we are interested in quasicrystals with atoms on their ideal positions only (without disorder).

[3] A map $f : A \to B$ is a bijection if it is both *one-to-one* (or *injective*) and *onto* (or *surjective*), *i.e.*, if two different elements $a_1, a_2 \in A$ have different image $f(a_1) \neq f(a_2)$ and if for each $b \in B$ there exists an $a \in A$ such that $f(a) = b$.

$A \subset B$ that A is a subset of B):

$$\begin{array}{ccccc} \mathbb{R}^d & \xleftarrow{\pi} & \mathbb{R}^d \times H & \xrightarrow{\pi_{\text{int}}} & H \\ \cup & & \cup & & \cup_{\text{dense}} \\ L & \xleftrightarrow{1-1} & \tilde{L} & \longrightarrow & L^* \end{array}$$

Looking at it differently, we have: The atoms are distributed on L, *i.e.*, the structure is a subset of L, and this subset intrinsically determines the internal space H and the lattice $\tilde{L}$.

For later reference, we define the so-called *star map* $^*: L \to H$, $x \mapsto x^* = \pi_{\text{int}}(\pi^{-1}(x))$, which is well-defined by the bijectivity of π on $\tilde{L}$ (*i.e.*, since L and $\tilde{L}$ are in one-to-one correspondence). Note that we have $\tilde{L} = \{(x, x^*) \mid x \in L\}$, *i.e.*, x^* is the internal coordinate for a point $x \in L$. See the following example for the use of the star-map.

Example: Cut-and-project scheme for the Penrose tiling

The rhombic Penrose tiling (see Figs. 1 and 6a)) has the following cut-and-project scheme (cf. [2] and [4, Section 5]): The direct space is $\mathbb{R}^2$ and the internal space is given by $H = \mathbb{R}^2 \times C_5$, where $C_5 = \mathbb{Z}/5\mathbb{Z}$ is the cyclic group of order 5. In the following, we think of C_5 as set $\{0, 1, 2, 3, 4\}$ with addition and multiplication modulo 5 – so it is in fact the finite field F_5. Here, the internal space is not purely Euclidean, but the interpretation in this case is not hard: We just have five copies of $\mathbb{R}^2$ as internal space.

For the lattice $\tilde{L}$, we use $\mathbb{R}^2 \simeq \mathbb{C}$ (*i.e.*, we identify the plane with the complex numbers $\mathbb{C}$) and set $\xi = \exp(2\pi i/5) = \cos(2\pi/5) + i \cdot \sin(2\pi/5)$. We define the following four vectors[4] $\boldsymbol{v}_1, \ldots, \boldsymbol{v}_4$ in $\mathbb{C}^2 \times C_5$:

$$\boldsymbol{v}_1 = \begin{pmatrix} 1 \\ 1 \\ 1 \end{pmatrix}, \qquad \boldsymbol{v}_2 = \begin{pmatrix} \xi \\ \xi^2 \\ 1 \end{pmatrix},$$

$$\boldsymbol{v}_3 = \begin{pmatrix} \xi^2 \\ \xi^4 \\ 1 \end{pmatrix} \quad \text{and} \quad \boldsymbol{v}_4 = \begin{pmatrix} \xi^3 \\ \xi \\ 1 \end{pmatrix},$$

which as vectors of $\mathbb{R}^4 \times C_5$ read

$$\boldsymbol{v}_1 = \begin{pmatrix} 1 \\ 0 \\ 1 \\ 0 \\ 1 \end{pmatrix}, \qquad \boldsymbol{v}_2 = \begin{pmatrix} \cos\left(\frac{2\pi}{5}\right) \\ \sin\left(\frac{2\pi}{5}\right) \\ \cos\left(\frac{4\pi}{5}\right) \\ \sin\left(\frac{4\pi}{5}\right) \\ 1 \end{pmatrix},$$

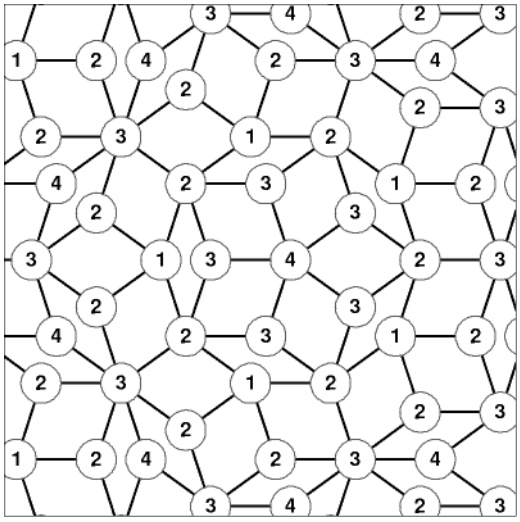

Fig. 1. A small section of the ideal Penrose tiling showing the numbering $\{1, 2, 3, 4\}$ of the vertices (*i.e.*, a 1-vertex is denoted by "1" etc.) as used in the text.

$$\boldsymbol{v}_3 = \begin{pmatrix} \cos\left(\frac{4\pi}{5}\right) \\ \sin\left(\frac{4\pi}{5}\right) \\ \cos\left(\frac{8\pi}{5}\right) \\ \sin\left(\frac{8\pi}{5}\right) \\ 1 \end{pmatrix} \quad \text{and} \quad \boldsymbol{v}_4 = \begin{pmatrix} \cos\left(\frac{6\pi}{5}\right) \\ \sin\left(\frac{6\pi}{5}\right) \\ \cos\left(\frac{2\pi}{5}\right) \\ \sin\left(\frac{2\pi}{5}\right) \\ 1 \end{pmatrix}.$$

The lattice $\tilde{L}$ is given as $\mathbb{Z}$-span of these four vectors (*i.e.*, as linear combination with integral coefficients), therefore

$$\begin{aligned} \tilde{L} &= \langle \boldsymbol{v}_1, \boldsymbol{v}_2, \boldsymbol{v}_3, \boldsymbol{v}_4 \rangle_{\mathbb{Z}} \\ &= \{h \cdot \boldsymbol{v}_1 + j \cdot \boldsymbol{v}_2 + k \cdot \boldsymbol{v}_3 + \ell \cdot \boldsymbol{v}_4 \mid h, j, k, \ell \in \mathbb{Z}\}, \end{aligned}$$

where we use addition modulo 5 in the C_5-component. The projection π projects $\tilde{L}$ on $L = \mathbb{Z}[\xi] = \{h + j \cdot \xi + k \cdot \xi^2 + \ell \cdot \xi^3 \mid h, j, k, \ell \in \mathbb{Z}\}$. The ring (of integers of the cyclotomic field of the fifth roots of unity) $\mathbb{Z}[\xi]$ is a rank 4 $\mathbb{Z}$-module with basis[5] $\{1, \xi, \xi^2, \xi^3\}$, which yields the bijectivity of $\pi: \tilde{L} \to L = \mathbb{Z}[\xi]$. The star map $^*: L \to \mathbb{C}^2 \times C_5$ for an element $x = h + j \cdot \xi + k \cdot \xi^2 + \ell \cdot \xi^3 \in \mathbb{C}$ is given[6] by $x^* = (h + j \cdot \xi^2 + k \cdot \xi^4 + \ell \cdot \xi, (h + j + k + \ell) \bmod 5)^T$ (by $(\cdot, \cdot)^T$ we denote the column vector one obtains by transposing the row vector $(\cdot, \cdot)$).

One also checks that L^* is dense in H (because each of the sets $S_m = \{h + j \cdot \xi^2 + k \cdot \xi^4 + \ell \cdot \xi \mid (h + j + k + \ell) \equiv m \bmod 5\}$ is dense in $\mathbb{C}$). We also have to check that $\tilde{L}$ is a lattice in $\mathbb{R}^4 \times C_5$. Mathematically, one has to check that $\tilde{L}$ is discrete and that the factor group $(\mathbb{R}^4 \times C_5)/\tilde{L}$ is compact. But here, the meaning of a lattice should be

[4] Since $\mathbb{C}^2 \times C_5$ is not a vector space, the $\boldsymbol{v}_i$'s are actually only triples not vectors. Nevertheless, since we are only interested in multiplying these objects by elements of $\mathbb{Z}$ (which is a well-defined operation), we prefer the name "vector" for such objects because it seems more suggestive.

[5] So every expression of the form $a_0 + a_1 \cdot \xi + a_2 \cdot \xi^2 + \ldots + a_N \cdot \xi^N$ with coefficients $a_0, \ldots, a_N \in \mathbb{Z}$ can (uniquely) be written as $h + j \cdot \xi + k \cdot \xi^2 + \ell \cdot \xi^3$ with coefficients $h, j, k, \ell \in \mathbb{Z}$.

[6] The star map consists of the Galois automorphism of $\mathbb{Z}[\xi]$ sending ξ to ξ^2 (observe that $\xi^6 = \xi$) and a homomorphism $\varrho: \mathbb{Z}[\xi] \to C_5$ defined by $\varrho(h + j \cdot \xi + k \cdot \xi^2 + \ell \cdot \xi^3) = (h + j + k + \ell) \bmod 5$.

clear if we forget the C_5-component, and we remark that we basically do not have to care about such a finite (and therefore compact) group for the lattice property.

Remark on the cut-and-project scheme for the Penrose tiling

Often, the cut-and-project scheme for the Penrose tiling is obtained by a 2-dimensional section through $\mathbb{R}^5$ (*i.e.*, one uses $\mathbb{R}^5$ for $\mathbb{R}^2 \times H$), see *e.g.* [23, 43, 31]. But this is just a special interpretation of the finite group C_5: In this case, $C_5 = \mathbb{Z}/5\mathbb{Z} = \{0,1,2,3,4\}$ is "embedded" into $\mathbb{R}$ by taking $z \in \{0,1,2,3,4\}$ as its coordinate in $\mathbb{R}$, yielding $\mathbb{R}^3$ as internal space. However, this interpretation is, from a mathematical point of view, unsatisfactory since we need the denseness of L^* in H in what follows.

2.2 Model sets

Given a cut-and-project scheme $(\mathbb{R}^d, H, \tilde{L})$ and a non-empty compact set $W \subset H$ in the internal space, which is the closure of its interior and which we call the *window*, we define the set

$$\Lambda(W) = \{x \in L \mid x^* \in W\},$$

i.e., the set of points x of $L \subset \mathbb{R}^d$ such that x^* is a point of the window. Then a set $\Lambda \subset \mathbb{R}^d$ is a *model set* or *cut-and-project set* for the cut-and-project scheme $(\mathbb{R}^d, H, \tilde{L})$ if $\Lambda = t + \Lambda(W)$ for some $t \in \mathbb{R}^d$, see [28].

Model sets always fulfil the first three properties **A1–A3** in the last section and they are also Delone sets. With regard to **A4**, we call a model set *regular* if the boundary ∂W of the window W has (Haar[7]) measure 0. Now we are able to state a sufficient condition for property **A4**.

Theorem 1. [30] *Regular model sets are pure point diffractive.* □

Furthermore, we say that a model set is *generic* if $L^* \cap \partial W \varnothing$ (*i.e.*, there are no points of L^* on the boundary of the window). For a *singular* (*i.e.*, non-generic) model set, one often explicitly states which points on the boundary ∂W are projected and which are not (see remark for the Penrose tiling below) to obtain the model set.

We also remark that one usually starts with a cut-and-project scheme and a window to obtain a model set. Here, however, the picture is different: We are given some point set in $\mathbb{R}^d$ with properties **A1–A4**, which implicitly defines the cut-and-project scheme and – if possible – also the window. From a conceptual perspective, this latter approach to model sets is more satisfying: The structure determines its description as a model set.

[7] The internal space H is (by construction) always a locally compact Abelian group and therefore one can define a measure on it which lines up with the group structure, called the Haar measure. On $\mathbb{R}^d$ the Haar measure coincides (up to a multiplicative constant) with the Lebesgue measure. A model set is therefore regular, if the boundary ∂W of the window does *not* consist of some exotic space-filling curve (in $\mathbb{R}^2$) or surface (in $\mathbb{R}^3$). Especially, if the window is some polygon or polyhedron, we always obtain a regular model set.

Example: Model sets and crystals

Set $H = \{0\} = W$ and let $L \subset \mathbb{R}^d$ be a lattice. Then $\tilde{L} = \{(x,0) \in \mathbb{R}^d \times \{0\} \mid x \in L\} \simeq L$, $x^* = 0$ for all $x \in L$ and $\Lambda(W) = L$. Therefore, lattices are model sets for a trivial cut-and-project scheme $(\mathbb{R}^d, \{0\}, \tilde{L})$. Furthermore, crystals can be regarded as finite union of translated copies of a lattice, therefore they may be interpreted as model sets where the internal space H is (at most) a discrete group or as a lattice with some decoration.

Example: The Penrose tiling as model set

Let P be the pentagon obtained as the convex hull of $\{1, \xi, \xi^2, \xi^3, \xi^4\}$ (*i.e.*, a regular pentagon of circumradius 1) and denote by aP ($a \in \mathbb{R} \setminus \{0\}$) the regular pentagon of circumradius $|a|$, which is reflected in the origin if $a < 0$. Set $W^{(1)} = P$, $W^{(4)} = -P$, $W^{(3)} = \tau P$ and $W^{(2)} = -\tau P$ (we might add $W^{(0)} = \varnothing$ for completeness). We set

$$W = \bigcup_{k=0}^{4} \begin{pmatrix} W^{(k)} \\ k \end{pmatrix} = \begin{pmatrix} P \\ 1 \end{pmatrix} \cup \begin{pmatrix} -\tau P \\ 2 \end{pmatrix} \cup \begin{pmatrix} \tau P \\ 3 \end{pmatrix} \cup \begin{pmatrix} -P \\ 4 \end{pmatrix},$$

and therefore have $W \subset \mathbb{C} \times C_5$. Then $\Lambda(W)$ is singular, *i.e.*, there are points of L^* on the boundary of W (where $\partial W = (\partial P, 1)^T \cup \ldots \cup (-\partial P, 4)^T$). By looking at $\Lambda(W)$ one easily recognises that there are too many points around the origin (*i.e.*, we get a point pattern that only appears around the origin in $\Lambda(W)$). One therefore states which boundary lines of the pentagons involved are used. As an equivalent alternative, we can also add a displacement $(\gamma, 0)^T \in \mathbb{C} \times C_5$ to W (*i.e.*, we translate all pentagons involved by γ), such that $\Lambda(W + (\gamma,0)^T)$ is generic (*e.g.*, $\gamma = \sqrt{7}$ is such a choice). Then $\Lambda(W + (\gamma,0)^T)$ is the set of vertex points of the (or better a) Penrose tiling. The tiling is obtained from the point set by connecting points of distance 1 to each other. If we denote a point x with $x^* \in (W^{(k)}, k)^T$ as k-vertex (where $k \in \{1,2,3,4\}$), then we have for the tiling: a 1-vertex has only edges to 2-vertices, and similarly, a 4-vertex has only edges to 3-vertices, while a 2-vertex (respectively a 3-vertex) can have edges to 1- and 3-vertices (respectively 2- and 4-vertices), see Fig. 1. In [43, 41], 1-, 2-, 3- and 4-vertices are called circle, square, triangle and star vertices, respectively.

2.3 Deformed model sets

Let $\theta : H \to \mathbb{R}^d$ be a continuous map (in fact, $\theta : W \to \mathbb{R}^d$ piecewise continuous[8] suffices) and $\Lambda(W)$ a regular model set. Then we can define the set

$$\Lambda_\theta(W) = \{x + \theta(x^*) \mid x^* \in W\} = \{x + \theta(x^*) \mid x \in \Lambda(W)\}.$$

[8] If $H = \mathbb{R}$, then θ is piecewise continuous if it is continuous on all but a finite number of points. More generally, we say that θ is piecewise continuous if it is made up of a finite number of continuous pieces.

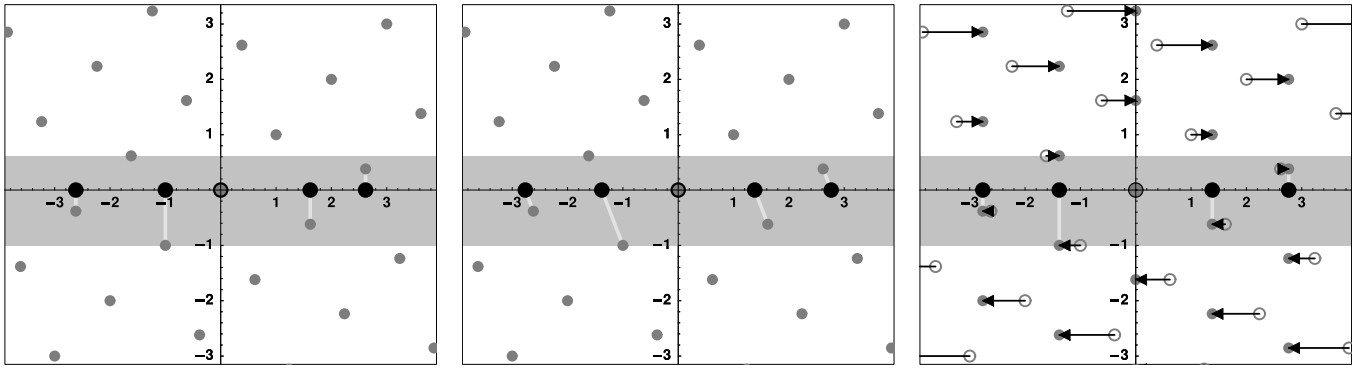

Fig. 2 (**a**) The Fibonacci chain is a model set: The lattice points $\tilde{L}$ are drawn in dark gray, while the window W defines the light gray strip. All lattice points which fall into this strip are projected (orthogonally) onto the horizontal axis, which yields the Fibonacci chain (black points). (**b**) The deformed Fibonacci chain i: Instead of using an orthogonal projection, we can also think of using a projection in direction $(1, -\tau^2)^T$ (noting that the deformation is $\theta(y) = y/\tau^2$). More precisely, we attach to every lattice point the function $-\theta^{-1}(y)$. The points of intersection with the horizontal axis yield the deformed model set. (**c**) Again the deformed Fibonacci chain i: To the obtain the deformed model set, we can also think of "deforming" the lattice by θ, *i.e.*, each lattice point (x, y) is shifted by $\theta(y)$ in the (horizontal) x-direction (the original lattice points are drawn as open circle; they are shifted to the filled points by θ). The new "lattice" points are then projected orthogonally as before.

We call $\Lambda_\theta(W)$ a *deformed model set* if it is still a Delone set (by the compactness of W, it is always relatively dense, only the uniform discreteness remains to be checked, *i.e.*, that **A1** is still fulfilled), see [12, 3].

Theorem 2. [12, Theorem 4.4] and [3, Theorem 6] *Deformed model sets are pure point diffractive.* □

This Theorem is quite remarkable, considering some of the following properties (especially v) of deformed model sets:

(i) By definition, deformed model sets are Delone sets.

(ii) The regular model set $\Lambda(W)$ is a deformed model set with deformation $\theta \equiv 0$.

(iii) A deformation does not change the density of the structure (see [3, Equation 12]), *i.e.*, dens $(\Lambda_\theta(W))$ = dens $(\Lambda(W))$.

(iv) The pure point spectrum (*i.e.*, the Bragg peaks) of the deformed model set $\Lambda_\theta(W)$ is concentrated on $\pi(\tilde{L}^*)$, *i.e.*, the support of the point spectrum is the same as the support of the regular model set $\Lambda(W)$. Here, $\tilde{L}^*$ denotes the dual or reciprocal lattice of $\tilde{L}$. Only the intensities (but not the locations) of the Bragg peaks change, if we compare the model set $\Lambda(W)$ with one of its deformed versions $\Lambda_\theta(W)$, see [12, Theorem 4.4].

(v) Unless θ is affine, *i.e.*, unless θ is a composition of a linear map and a translation, the set of inter-atomic distances $\Delta = \{x - y \,|\, x, y \in \Lambda_\theta(W)\}$ of a deformed model set is – contrary to the model set $\Lambda(W)$ – not a Delone set. This might be counter-intuitive for a crystallographer who has only dealt with crystals so far: We can have deformations such that the lengths of the inter-atomic distances are dense in an interval, but the diffraction spectrum is still only pure point diffractive (and has no continuous or diffuse component), also see the first example below. This property also indicates that assumption **A3** is not necessary to get pure point diffractivity!

(vi) The Fourier-Bohr coefficient $c_k(\Lambda_\theta(W))$ at $k \in \pi(\tilde{L}^*)$ (and therefore the intensity $|c_k|^2$ of the Bragg peak at this k) is given by

$$c_k = \frac{1}{\mathrm{vol}\,(\tilde{L})} \int_W \exp\left(-2\pi i \cdot (\langle k, \theta(y)\rangle - \langle k^*, y\rangle)\right) \mathrm{d}y\,,$$

where vol $(\tilde{L})$ denotes the volume of the fundamental domain of $\tilde{L}$, and $\langle \cdot, \cdot \rangle$ the scalar product. This formula is given in [20, Theorem 3.3] and [12, Theorem 2.6] if $H = \mathbb{R}^m$. If H is a more general space, this formula has to be interpreted in terms of the Haar integral and the appropriate scalar product. Note that $c_0 = \mathrm{dens}\,(\Lambda_\theta(W))$.

So the deformation specifies the intensities of the Bragg peaks, while their position is already determined by the underlying regular model set which is deformed. But we remark that the inverse problem is (as so often in crystallography) much harder: neither do the positions of the Bragg peaks determine the underlying model set – different model sets can have Bragg peaks at the same positions – nor do the intensities specify the deformation (trivially, we can always add a constant vector to θ which just has the effect of a translation in direct space, but no effect on the diffraction pattern).

Examples of deformed model sets are given in [12, Section 5], [10] (also see [33]) and [3, Section 6].

Example: Deformed Fibonacci chains

This example is taken from [12, Section 5]: The one-dimensional Fibonacci chain[9] can be described as model set with lattice $\tilde{L} \subset \mathbb{R}^2$ generated by $\boldsymbol{v}_1 = (\tau, 1-\tau)^T$ and $\boldsymbol{v}_2 = (1, 1)^T$ and window $W = [-1, \tau - 1[\subset \mathbb{R}$ (where $\tau = (1+\sqrt{5})/2$ is the golden mean), see Fig. 2a). Nearest neighbours of this model set are separated by the lengths $\pi(\boldsymbol{v}_2) = 1$ and $\pi(\boldsymbol{v}_1) = \tau$.

[9] Usually the Fibonacci chain is obtained by the substitution rule $a \mapsto ab$ and $b \mapsto a$ which yields $a \mapsto ab \mapsto aba \mapsto \ldots \mapsto abaababaab \ldots$ and therefore the sequence $abaababaab \ldots$. Then each a is represented by an interval of length τ and each b by one of length 1.

We now deform this Fibonacci chain with some specific deformations θ:

(i) $\theta(y) = y/\tau^2$: If θ is an affine function (especially, if it is linear), the nearest neighbours are separated by $\ell_k^{(\theta)} = \pi(\boldsymbol{v}_k) + \theta(\pi_{\text{int}}(\boldsymbol{v}_k)) - \theta(0)$. For the θ considered here, we get $\left(\text{by observing } \tau = 1 + \frac{1}{\tau}\right)$ $\ell_1^{(\theta)} = \tau + \frac{1-\tau}{\tau^2} - 0 = 1 + \frac{1}{\tau^2} = 1 + \frac{1}{\tau^2} - 0 = \ell_2^{(\theta)}$, *i.e.*, $\ell_1^{(\theta)} = \ell_2^{(\theta)}$. Therefore, all nearest neighbour distances are equal, wherefore we simply get a one-dimensional lattice with lattice constant $\ell_1^{(\theta)}$. We visualise this deformation in a "cut-and-project scheme" in Figs. 2b) and 2c).

(ii) $\theta(y) = \frac{1}{2}y^2$: In the general case, the nearest neighbours are separated by $\ell_k^{(\theta)} = \pi(\boldsymbol{v}_k) + \theta(y + \pi_{\text{int}}(\boldsymbol{v}_k)) - \theta(y)$ where $y, y + \pi_{\text{int}}(\boldsymbol{v}_k) \in W$, *i.e.*, the lengths depend on the internal coordinate y. For the θ considered here, we get $\ell_1^{(\theta)} = (1-\tau)\cdot y + \frac{1}{2}(\tau+2)$ with $y \in [\tau-2, \tau-1[$ and therefore $\ell_1^{(\theta)} \in]\frac{3}{2}\tau - 1, \frac{5}{2}\tau - 2]$. Similarly, we get $\ell_2^{(\theta)} \in [\frac{1}{2}, \tau - \frac{1}{2}[$. We observe that no two nearest neighbour distances are equal (a similar statement holds for arbitrary atomic distances in this deformed model set), but their values are dense in two nontrivial intervals, so clearly the set of interatomic distances Δ is not a Delone set. Still, this deformed model set is pure point diffractive!

Remark: Deformed model sets and crystals

As pointed out in Section 2.2, lattices can be described as model sets with a trivial cut-and-project scheme $(\mathbb{R}^d, \{0\}, \tilde{L})$. However, with such an internal space $H \simeq \{0\}$, a deformation θ amounts just to an overall translation of the whole lattice in $\mathbb{R}^d$. Similarly, interpreting a crystal as a model set, a deformation may change the decoration (*i.e.*, the position of the atoms) in the unit cell (wherefore the symmetry of the crystal may change), but not the property of being a crystal. For aperiodic model sets (*e.g.*, the Penrose tiling) the situation can be more drastic: Every regular model set is *repetitive*, *i.e.*, given a (finite) local configuration S in the model set, there is a radius R_S such that a translate of the configuration S is found in every ball of radius R_S (so this is a weak version of the periodicity inherent to crystals). But a deformed model set may not be repetitive anymore (see the deformation for the Fibonacci chain discussed in ii above), in fact, every(!) local configuration may only appear once in the whole structure.

Remark: Deformation in Section 3 (below)

In the cited literature ([12], [10] and [3]), the following procedure is used: Given a regular model set, one chooses a specific deformation θ to obtain a deformed model set with some specific properties. In this article, we use a different approach: We have a structure S – here a distorted Penrose tiling – which is obtained by some procedure (*e.g.*, a Monte Carlo simulation) from a (regular) model set Λ. We then ask whether this structure can be described as a deformed model set, *i.e.*, whether we can find a continuous function θ such that Λ_θ is (in some sense) a good approximation for S.

2.4 Disorder

There are two basic scenarios of disorder for point sets (not necessarily lattices or model sets): Either (possibly different) atoms[10] are distributed at random on the point set, or the atoms are displaced randomly from their ideal positions. We briefly review both scenarios, which were treated under quite general assumptions on the underlying point set in [26].

If the atoms are distributed at random (and especially independent between the sites) on the point set [26, Model A] (also see [5]), one models a random solid solution/an alloy. The lattice case was already treated by Laue, but the result remains qualitatively the same for a general point set: The diffraction spectrum consists (almost surely) of two terms; the first one describes the diffraction spectrum of a system where the scattering amplitudes have been replaced by their mean (which for lattices and model sets is pure point diffractive), while the second term is a homogeneous diffuse background which is proportional to the mean square difference of the scattering amplitudes.

We now explain the effect of random displacements on the diffraction pattern, which describes the effect of thermal motion in the Einstein approximation of the solid [26, Model B] (see [19] for model sets, for lattices/crystals this is the well-known Debye-Waller effect), and therefore the X-ray diffraction of the structure at high temperature. This is mathematically modeled if we replace the set of position for the atoms Λ by

$$\Lambda^{(\omega)} = \{x + \omega_x \mid x \in \Lambda\},$$

where ω_x are random displacements (taking values in $\mathbb{R}^d$), which are assumed to be bounded (in fact, a finite expectation value suffices, see [19, Theorem]), independent from each other over the sites $x \in \Lambda$, and have the same distribution ω (*i.e.*, the random variables ω_x are independent and identically distributed (abbreviated i.i.d.)).

For this kind of disorder, the well-known Debye-Waller factor is recovered: If we denote the Fourier transform of ω by $\hat{\omega}$, then the disorder (here, we may think of the disorder which arises from thermal motion) described by ω has (almost surely) two effects on the diffraction spectrum. Firstly, the diffraction pattern of the original structure Λ is reduced by the envelope function $|\hat{\omega}|^2$, which is 1 at the origin and tends to zero (although not necessarily monotonically) with increasing distance from the origin if ω is non-singular. Secondly, an absolutely continuous spectral component (*i.e.*, the diffuse scattering due to thermal motion) is added, which is described by the function $(1 - |\hat{\omega}|^2) \cdot \text{dens}(\Lambda)$. Therefore, we get "lots" of diffuse scattering in regions where the intensities of the Bragg peaks are reduced "a lot" due to thermal motion. We remark that, if we allow for i.i.d. Gaussian displacements

[10] with holes interpreted as "zeronium"

ω_x, then $|\hat{\omega}|^2$ is again a Gaussian (the temperature dependence is hidden in the variance of ω).

Remark: Deformation vs. random displacements

We can model displacements in a model set, *i.e.*, deviations from the ideal atom positions $\Lambda(W)$, in two ways (also compare to [20, Section 4.3.1]): Either they are random and we get $\Lambda^{(\omega)}$ or they can be described by a deformation θ and we have Λ_θ. In both cases, the location of the Bragg peaks remains the same, only their intensity changes. For random displacements, *i.e.*, in the Debye-Waller scenario, we usually always have a reduction of the intensities (with the exception of the central peak), while a deformation can increase some intensities and decrease others (*e.g.*, we also can have total extinction of some peaks). Furthermore, deformed model sets are still pure point diffractive, while we get diffuse scattering if there is some disorder present.

2.5 The size effect in crystals

Of course, from an experimental point of view, it would also be interesting to allow for a distribution (short-range order) and displacements of the atoms which depend on the neighbourhood. These effects, especially the latter one, have been treated for (conventional) crystals in [35], also see [18, 36, 13, 37] and references therein (for comparisons with experimental data, cf. [38, 14, 42, 39, 25]).

Both effects give modulations in the diffuse scattering (the Bragg peaks are unchanged). The effect of short-range order (where the atoms are assumed to stay at their ideal positions, but the occupation is determined by the neighbourhood) is a cosine periodic modulation in reciprocal space ("cosine" implies that it is symmetric around Bragg peaks). The size effect, *i.e.*, where relaxations take place locally (neighbouring atoms tend to move apart if they are both large, or closer together if they are both small), yields sine modulations which increase in magnitude with increasing distance from the origin. The size effect (re-)distributes the diffuse intensity such that there is more on one side of each Bragg peak and less on the other side; for (calculated) pictures of this property see [36] and Fig. 3. In the case of a two component alloy, we have the following: If the atom with the large scattering power is also the larger in size, the wings about a Bragg peak are high on the small angle side and low on the large angle side. When the atom with the higher scattering is smaller in size, the wings about a Bragg peak are low on the small angle side and high on the large angle side, see Fig. 3. Therefore one obtains a very characteristic feature in the diffraction pattern: The intensity of diffuse scattering is diminished on one side of a plane that passes through Bragg peaks and is enhanced on the other. So for crystals, we speak of a size-effect intensity transfer that operates on the diffuse scattering. Also we remark that one needs (two) different types of scatterer to be present.

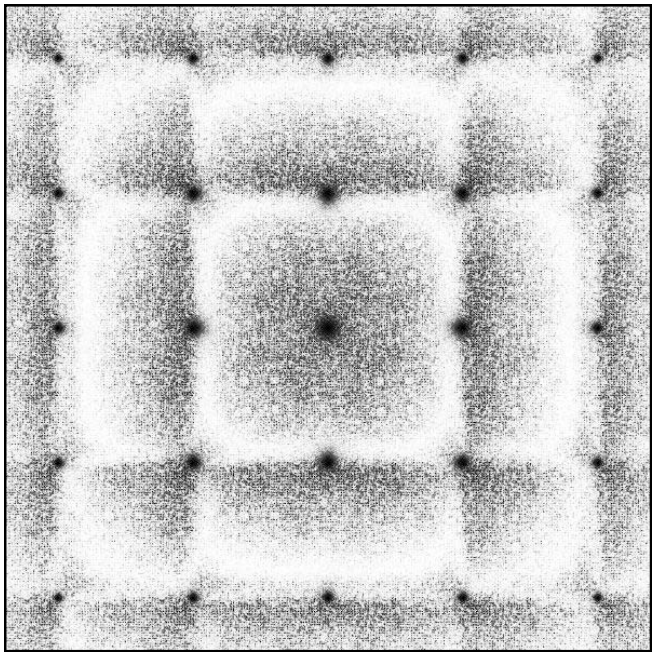

Fig. 3. An example pattern which demonstrates the size effect in a cubic two-component alloy: The smaller atom has the higher scattering power. The diffraction pattern is calculated with DISCUS [29].

Remark: Short-range order in quasicrystals

The main focus of this article in Section 3 will be on size-effect-like displacements, therefore we only remark on the role of short-range order, *i.e.*, a distribution of the atoms which depends on the neighbourhood, in quasicrystals. The diffraction of such a structure, a so-called random tiling [17], has not been treated rigorously so far. But there is very good evidence based on scaling arguments and extensive numerical investigations (see [17, 21] and references therein) that the situation is different for random tiling diffraction with non-crystallographic symmetry in two dimensions (while it is the same in three dimensions as in the lattice case): the diffraction spectrum is believed to have a singular continuous part (neither pure point diffractive/Bragg peaks nor diffuse/absolutely continuous) in this case, which is usually not considered in classical crystallography. For random tilings, $d = 2$ seems to be a critical dimension w.r.t. diffractive properties [17], since one-dimensional random tilings have absolutely continuous spectrum [8], while higher dimensional ($d \geq 3$) random tilings seem to possess Bragg peaks. But there is still no rigorous proof for this claim (also see [1, 11] and references therein).

Remark: Mutual local derivability (MLD)

The long-range order in crystals is characterised by the underlying space group. For long-range order, the decoration of the unit cell is not important, one is only interested in structures of the same space group. Note that it is difficult to formulate a concept for the space group for a quasicrystal in $\mathbb{R}^d$ without referring to the higher dimensional embedding space $\mathbb{R}^d \times H$. [The Fourier approach [27] is strictly equivalent to the approach via the embedding space [16].] Of course, in the quasicrystalline case one is also interested, if two structures are the same up to decoration. This is formalised by the concept of *mutual local*

derivability (MLD), see [9]. A discrete structure S_1 is *locally derivable* from the discrete structure S_2, if there is a radius $r \geq 0$, such that for all points $x \in \mathbb{R}^d$ and every vector t we have

$$S_2 \cap B_r(x) = S_2 \cap B_r(x+t) \Rightarrow S_1 \cap \{x\} = S_1 \cap \{x+t\},$$

where $B_r(x)$ denotes the ball of radius r around x. Therefore, S_1 is locally derivable from S_2, if points with the same neighbourhood (in a ball of radius r) in S_2 induce the same local configurations in S_1. If S_2 is also locally derivable from S_1, then S_1 and S_2 are mutually locally derivable.

We remark that structures which are MLD with a regular model set are also pure point diffractive. Furthermore, we observe that the following (deterministic) procedure yields a point set which is MLD to the original structure: Displace each vertex from its ideal position by a small distance which is determined only by its neighbours which are at most at distance r. This is a first approximation on the size-effect, but it does not take into account that the local shifts in the size-effect are transmitted to more distant neighbours and the relaxation spreads throughout the lattice to minimise the overall strain. This effect is much better incorporated in the concept of a deformed model set, where even weak influences of vertices which are far away can be included (the above procedure, which yields MLD point sets, can also be described in the case of model sets by a deformation θ which is piecewise constant).

Remark: Disorder in Section 2.4 and in this section

We again emphasise that the effects discussed in 2.4, like the Debye-Waller effect, yield qualitatively the same results in the diffraction pattern for quite a general class of point sets and could therefore be treated in this full generality in [26]. For the effects discussed in this section, things are different: the results discussed here only apply for crystals/lattices. In Section 3 we will argue that for size-effect-like displacements in the Penrose tiling we have persistence of pure point diffraction as observed and conjectured in [41]. This pure point diffractivity is understood by describing the structure as a deformed model set.

3. Distorted Penrose tilings

3.1 The model

We utilise the description of the rhombic Penrose tiling given in Section 2 to derive a two-dimensional tiling from the point set $\Lambda(W)$ (here, the two characteristic tiles for the Penrose tiling are obtained by connecting points of distance 1 to each other: a fat and a thin rhombus), see Fig. 6a) for a small region of the Penrose tiling. We classify the rhombus edges by the vertices they join and get just 3 different types: 1-vertex-2-vertex edges, 2-vertex-3-vertex edges and 3-vertex-4-vertex edges (with occurrences in the ratios 1 : 2 : 1 in the infinite tiling). We will use the abbreviations 1-2-edges, 2-3-edges and 3-4-edges respectively.

After generating a large (circular) region of the rhombic Penrose tiling containing 127 959 vertices[11] (of which 1 129 are boundary vertices and are kept fixed during the Monte Carlo simulation), we have carried out a Monte Carlo (MC) simulation as in [41]. A Hooke's law spring is assumed to act along each rhombus edge with the equilibrium length of the springs given by $(1+\varepsilon)$ for 1-2-edges and 3-4-edges, respectively of length $(1-\varepsilon)$ for 2-3-edges (therefore, there is no net change of the average rhombus edge length). Various values for ε are used, here we will concentrate on $\varepsilon = +.15$. An MC energy of the form

$$E = \sum_{\text{edge}\{i,j\}} k_{\{i,j\}} \cdot (d(i,j) - (1+\varepsilon_{\{i,j\}}))^2$$

is used, where $d(i,j)$ is the instantaneous length of the rhombus edge $\{i,j\}$ connecting vertices i and j, $\varepsilon_{\{i,j\}} = \pm\varepsilon$ depending on the type of the edge $\{i,j\}$ (the $+$-value is used for 1-2-edges and 3-4-edges) and all springs are assumed to have the same strength $k_{\{i,j\}} = 1$. This is a toy model where 2-vertex and 3-vertex atoms tend to move together, while 1-vertex (respectively 4-vertex) and 2-vertex (respectively 3-vertex) atoms move apart, which is a size-effect-like behaviour.

The MC simulation is carried out by selecting a vertex at random and comparing the energy before and after a small random shift is applied to the position. The shift is accepted if the energy is lower and otherwise it is rejected with high probability, *i.e.*, a Boltzmann factor at very low temperature ($k_B T = .000\,005$) is used. Iteration is continued for 1 500 MC cycles (or sweeps), where a cycle is defined as the number of individual MC steps required to visit each vertex once on average. The progress of the MC is monitored by calculating the energy-loss per MC cycle, as well as by various averages, such as the mean lengths for the different types of rhombus edges. We call the result of such a MC simulation a *distorted Penrose tiling*.

3.2 The window revisited

There are two types of connected window-components, both occur in two different orientations: a small pentagon P (respectively $-P$) for 1-vertices and 4-vertices and a big pentagon τP (respectively $-\tau P$) for 2-vertices and 3-vertices. If for a vertex x one knows the location of x^* in these pentagons, one also knows to how many neighbouring vertices this vertex x is connected by an edge, see Fig. 4 (also compare to [2, Fig. 5.1]). To be more precise, these regions give exact information on the (next-nearest) neighbourhood of the vertex considered, see Fig. 5 (compare to [2, Fig. 5.2]). One can further divide the regions to obtain information about bigger parts of the neighbourhood (second and higher nearest neighbours).

Therefore vertices x and y, which have the same neighbourhood up to a certain radius, have internal coordinates x^* and y^* which are in the same (sub-)region, *i.e.*, which are close in internal space. Of course, in the spring model

[11] The 127 959 vertices used here yield 63 698 1-2-edges, 127 377 2-3-edges and 63 712 3-4-edges and therefore the ratios 1.000149 : 2 : 1.000369.

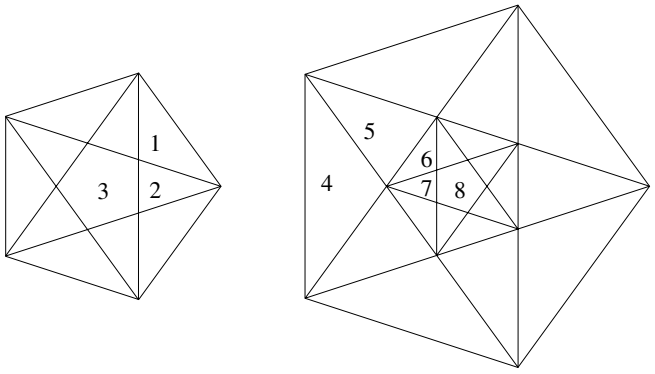

Region No.	1	2	3	4	5	6	7	8
No. of neighbours	3	4	5	3	5	7	6	5

Fig. 4. Regions in the small and big pentagon.

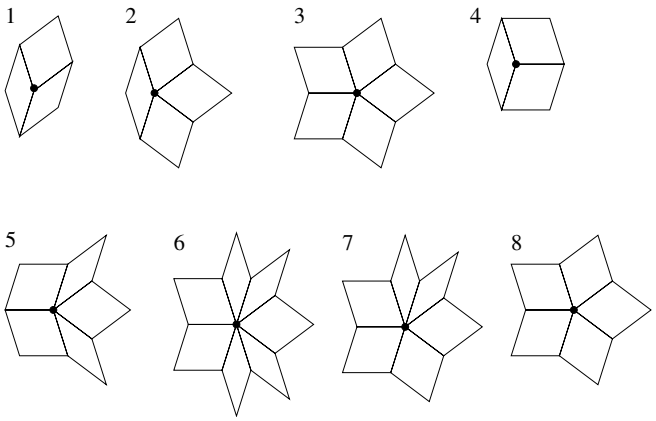

Fig. 5. Neighbourhood of a vertex (modulo rotation) which belongs to the specified region.

considered here (what we call a distorted tiling), the neighbourhood determines the displacement from the ideal position of a vertex. And so we may expect that if the internal coordinates x^* and y^* are in the same (sub-)region, then the vertices x and y show similar displacements. But this is (in an informal way) exactly what a deformed model set is: The displacement of a vertex from its ideal position x in direct space depends in some regular way (*i.e.*, continuously) on its internal coordinate x^*.

These considerations already suggest that distorted Penrose tilings might be well described as deformed Penrose tilings and that there will be persistence of pure point spectra.

3.3 Averaging

For a distorted Penrose tiling, we know for each vertex its distortion from its ideal position in the (undistorted/ideal) Penrose tiling. Since there is also some randomness present in MC simulations, we have averaged the distortions for each vertex over 500 distorted Penrose tilings, *i.e.*, we have run the MC simulation 500 times and then averaged for each vertex the 500 final coordinates. We call the outcome of this averaging process the *averaged distorted Penrose tiling.*

3.4 Calculation of the diffraction patterns

Diffraction patterns were calculated from the final positions of the vertices using the program DISCUS [29]. A single atomic scatterer was placed at each vertex. Calculations were made on a grid of 2400×2400 pixels and subsequently reduced to 600×600 by pixel averaging. For studying the system behaviour, the total 127 959 vertices were used in calculations of the diffraction patterns. However, for the purpose of illustration in this article, calculations were made using a smaller circular region of the tiling patterns containing approximately 10 500 vertices since in the former patterns the Bragg peaks were so small that they did not reproduce satisfactorily. The quadratic part of the diffraction patterns we show here, corresponds to the part where the reciprocal coordinates range from -2.4 to 2.4 (note that a rhombus edge in the ideal Penrose tiling has length 1). The diffraction pattern of the ideal Penrose pattern is shown in Fig. 6b).

3.5 Functions for deformation

We will represent a deformation θ for the Penrose tiling as follows: By definition, $\theta : \mathbb{C} \times C_5 \to \mathbb{C}$, but we already noted that we are actually only interested in a (piecewise) continuous function $\theta : W \to \mathbb{C}$ (which we again denote by θ). And finally, by the C_5-part of H, a deformation of the Penrose tiling is given by 4 (piecewise) continuous functions $\theta_k : W^{(k)} \to \mathbb{C}$ where $1 \leq k \leq 4$ (for the definition of $W^{(k)} \subset \mathbb{C}$, see p. 624).

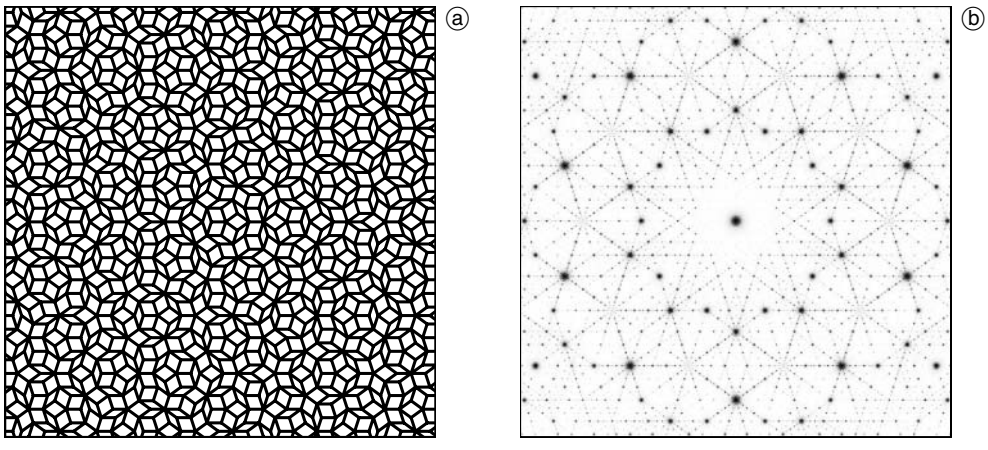

Fig. 6 (**a**) Part of the ideal Penrose tiling. (**b**) Diffraction pattern of the ideal Penrose tiling.

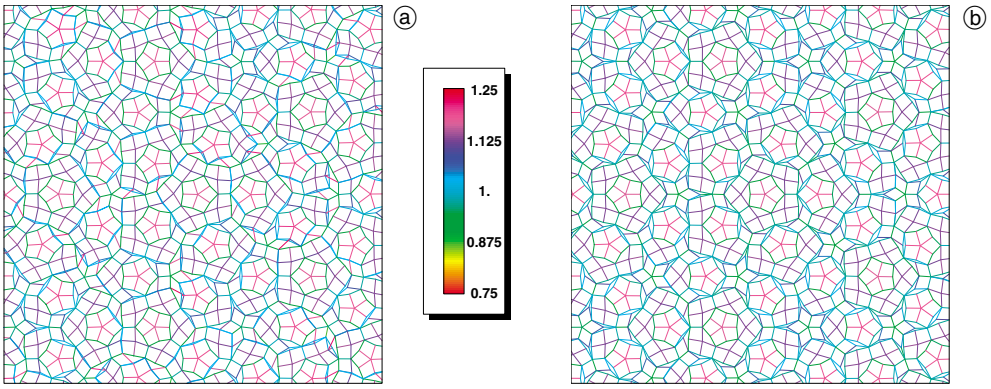

Fig. 7. Part of (**a**) a distorted Penrose tiling and (**b**) the averaged distorted Penrose tiling. The rhombus edges are coloured according to their length.

We write every such θ_k as $\theta_k(z) = r_k(z) \cdot e^{i \cdot \phi_k(z)}$, where $r_k(z) = |\theta_k(z)|$ is obtained by the complex modulus (or complex norm) from θ_k and $\phi_k(z) = \mathrm{Arg}\,(\theta_k(z))$ by the complex argument (*i.e.*, the phase) from θ_k. [If we use $\mathbb{R}^2 \simeq \mathbb{C}$, then we have $\theta_k(x, y) = (r_k(x, y) \cdot \cos(\phi(x, y)), r_k(x, y) \cdot \sin(\phi(x, y)))$.] Therefore, we have $r_k : W^{(k)} \to \mathbb{R}_{\geq 0}$ and $\phi_k : W^{(k)} \to]-\pi, \pi]$. We call r_k the *norm* and ϕ_k the *phase* of the deformation θ_k. If θ_k is continuous, then r_k is also continuous and ϕ_k is continuous if regarded as function modulo 2π (and the possible exception of points $z \in \mathbb{C}$ where $\theta_k(z) = 0 = r_k(z)$ and one therefore cannot define the complex argument; we set $\phi_k(z) = 0$ at such points).

Now for a distorted Penrose tiling, we proceed as follows: To the vertex ℓ (we enumerate the vertices of the tiling by ℓ) at position $z_\ell^{(2)} \in \mathbb{C}$ in the distorted Penrose tiling, we also know its position $z_\ell^{(1)} \in \mathbb{C}$ in the ideal (undistorted) Penrose tiling and its type i_ℓ, *i.e.*, if it is an i_ℓ-vertex ($i_\ell \in \{1, 2, 3, 4\}$). Writing $z_\ell^{(2)} = z_\ell^{(1)} + (z_\ell^{(2)} - z_\ell^{(1)})$, we are therefore looking for (piecewise) continuous functions $\theta_{i_\ell} : W^{(i_\ell)} \to \mathbb{C}$ such that they (ideally) describe the distortions, *i.e.*, that (ideally) $\theta_{i_\ell}((z_\ell^{(1)})^*) = z_\ell^{(2)} - z_\ell^{(1)}$ for all vertices ℓ in the tiling. Of course, by the inherent disorder in an MC simulation, we are not expecting this last equality to hold, but we hope that we can fit functions θ_k well to the obtained distortions.

Since we separate each function θ_k in its norm r_k and its phase ϕ_k, we make the following plots: Given $z_\ell^{(2)}$, $z_\ell^{(1)}$ and i_ℓ, we associate to the point $(z_\ell^{(1)})^* \in W^{(i_\ell)}$ in one plot the norm $|z_\ell^{(2)} - z_\ell^{(1)}|$ and in a second plot the phase $\mathrm{Arg}\,(z_\ell^{(2)} - z_\ell^{(1)})$ of the distortion for each of the ℓ vertices. These plots enable us to assess whether it would be feasible to fit some (piecewise) continuous functions r_k and ϕ_k to explain them.

Note that by the symmetry of the Penrose tiling, it is justified to expect that $\theta_1(z) = -\theta_4(-z)$ (*i.e.*, $r_1(z) = r_4(-z)$ and $\phi_1(z) = -\phi_4(-z)$) and $\theta_2(z) = -\theta_3(-z)$. Therefore, it suffices to plot the norm and the phase for the 1-vertices (and not also for the 4-vertices), respectively for the 3-vertices (and not also for the 2-vertices). In fact, we will use the relation $\theta_1(z) = -\theta_4(-z)$ to plot both, 1- and 4-vertices, over the same pentagon (and the same for 2- and 3-vertices).

3.6 Results

Small regions for the tiling patterns are shown in Fig. 6a) for the (ideal) Penrose tiling (all rhombus edges have length 1), in Fig. 7a) for a distorted tiling and in Fig. 7b) for the averaged distorted tiling. In the latter two cases, we have coloured the rhombus edges according to their lengths, compare to [41, Fig. 6].

Averaged distorted Penrose tiling

We first look at the averaged distorted Penrose tiling: The distinct colouring in Figs. 8b), 8d), 9b) and 9d) shows that the averaged distortions can be well described by piecewise continuous functions r_1, r_4 (Fig. 8b)), ϕ_1, ϕ_4 (Fig. 8d)), r_2, r_3 (Fig. 9b)) and ϕ_2, ϕ_3 (Fig. 9d)). We are not trying to actually find these functions by a fitting procedure here, since the observed patterns (see especially Figs. 9b) and 9d)) are quite complicated (although symmetrical). As an example, we look at region no. 2 of Fig. 4, and plot for all vertices ℓ which fall into this region (*i.e.*, if $(z_\ell^{(1)})^*$ is in region no. 2) the norm of the distortion (*i.e.*, $|z_\ell^{(2)} - z_\ell^{(1)}|$ in the notation of the last section) vs. the distance of that point in internal space from the origin of the pentagon (*i.e.*, vs. $|(z_\ell^{(1)})^*|$), see Fig. 11b). With a more carefully chosen parameter than just the distance from the origin in mind, it should be clear that one can (in principle) easily fit the norm in this region.

We summarise our findings for the averaged distorted Penrose tiling as follows: The averaged Penrose tiling (or the average structure of a distorted Penrose tiling) is rather well described as a deformed model set!

Distorted Penrose tiling

We now look at the distorted Penrose tiling: Here the colouring in Figs. 8a), 8c), 9a) and 9c) does not look as smooth as in the averaged case. Of course, this is often due to the inherent disorder present in MC simulations, and a comparison with the averaged distorted Penrose tiling often shows that the two match quite well in norm and phase. The effect of the averaging procedure can be seen by comparing Figs. 11a) and 11b), where we plot for region no. 2 the norm of the distortion vs. the distance from the origin. But there are also regions, like regions no. 1 and 5 in Fig. 4, where the correspondence to the averaged case is rather poor. For (many of) these vertices, the history of the MC simulation in the neighbourhood seems to play an important role, especially at this quite large value for ε of 0.15, see Section 3.7.

Ideally, we would like to describe a distorted Penrose tiling as a deformed Penrose tiling plus some random displacements. Of course our discussion shows that the "ran-

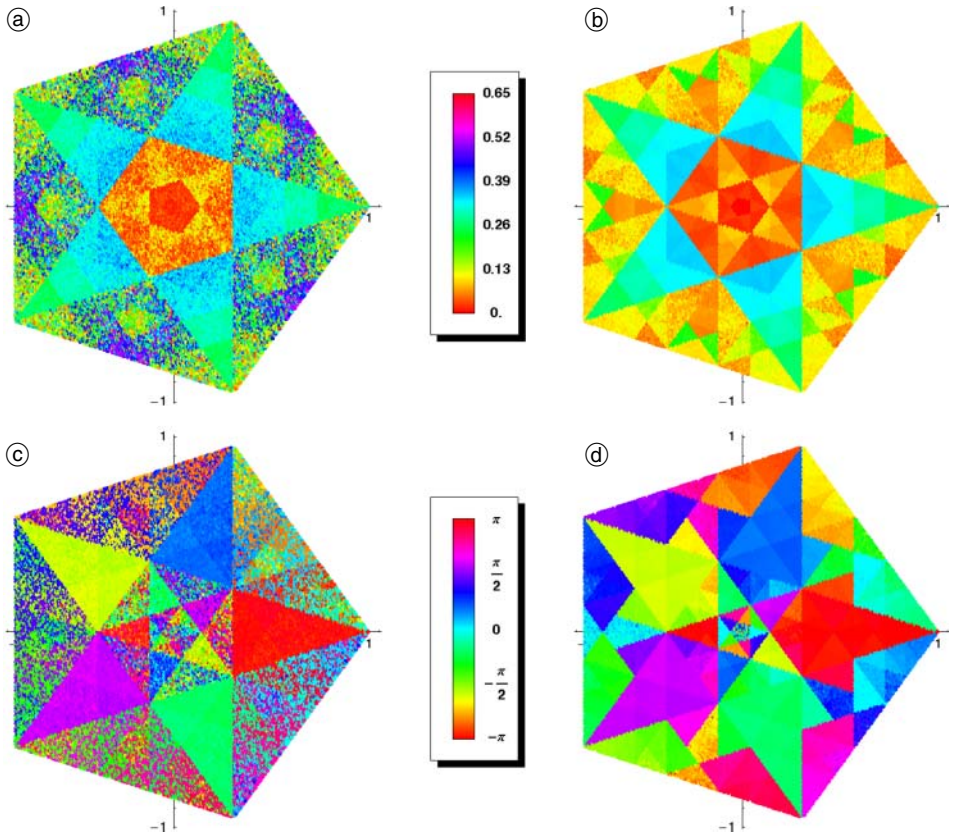

Fig. 8. (**a**) Norm of the distortions for 1- and 4-vertices. (**b**) Norm of the averaged distortions for 1- and 4-vertices. In both cases the same colour coding is used. (**c**) Phase of the distortions for 1- and 4-vertices. (**d**) Phase of the averaged distortions for 1- and 4-vertices. For the phase, the same colour coding is used in both cases.

dom" displacements here are (at least for atoms of region no. 1 and 5) correlated to the positions of the atoms in their neighbourhood, see also the distribution of bond lengths in Section 3.7 (Fig. 12).

However, we claim that the Bragg part of the diffraction pattern can be well explained on the basis of deformed model sets. Indeed, if we look at the Bragg peaks in the diffraction pattern of a distorted Penrose tiling as in Fig. 10a), we see that they are essentially the same (in position and intensity) as the Bragg peaks of the averaged distorted Penrose tiling in Fig. 10b) – which by the above discussion is basically the diffraction pattern of a de-

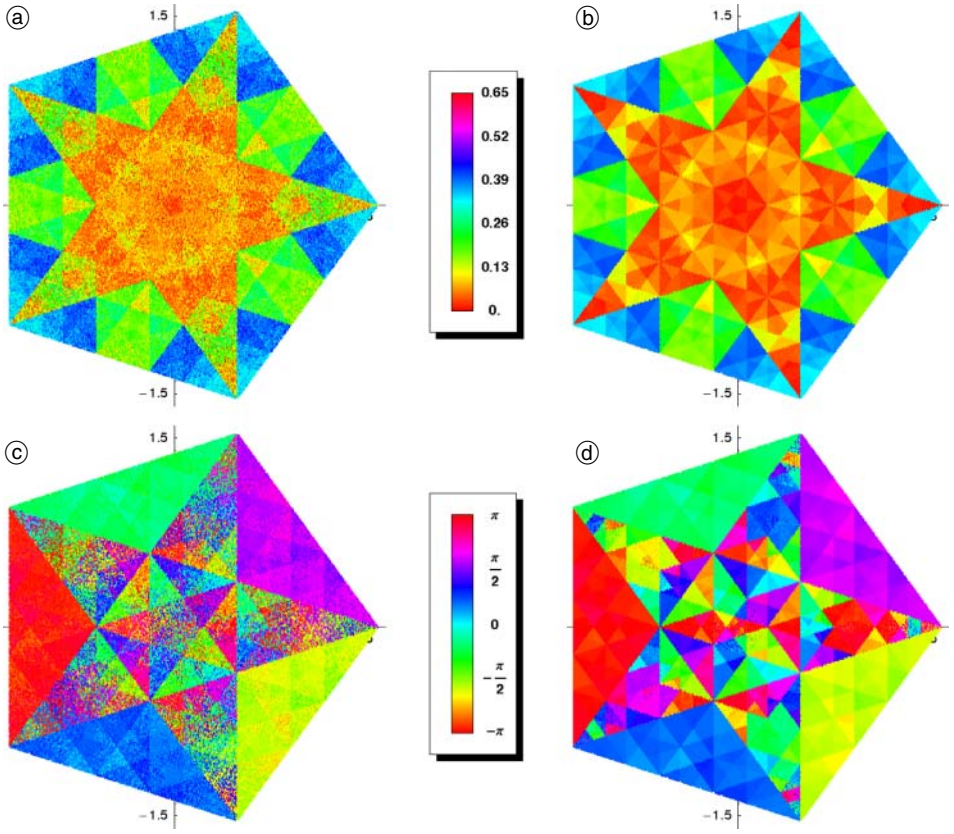

Fig. 9. (**a**) Norm of the distortions for 2- and 3-vertices. (**b**) Norm of the averaged distortions for 2- and 3-vertices. As before, the same colour coding is used in both cases. (**c**) Phase of the distortions for 2– and 3-vertices. (**d**) Phase of the averaged distortions for 2- and 3-vertices. Again, c) and d) use the same colour coding for the phase.

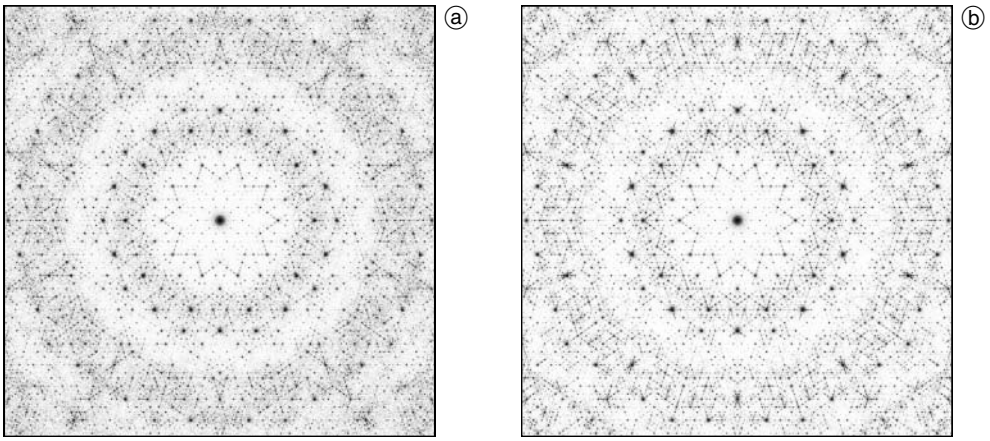

Fig. 10. Diffraction pattern of (**a**) a distorted Penrose tiling and (**b**) the averaged distorted Penrose tiling.

formed model set and therefore has (almost) no diffuse scattering. Furthermore, we observe – as already recognised in [41] – that there are decagonally shaped features with delineated boundaries separating an inner region of low intensity from an outer region of high intensity. There is also a second circular band of lower intensity outside the strong band, and another band of strong intensity.

By this observation, we can emphasise once more that for the size-effect-like displacements in the distorted Penrose tiling we have persistence of pure point diffraction, and there is an intensity transfer that operates on the Bragg peaks. This parallels the situation for the size effect in crystals, only there the intensity transfer affects the diffuse scattering. These findings should provide an explanation for the experimental data in [15].

3.7 Further investigations

We show in Fig. 12 plots of the frequency with which rhombus edges occur in a distorted Penrose tiling and in the averaged distorted Penrose tiling respectively (cf. [41, Fig. 5]). In the averaged case this distribution is more "spiky", which is clear by looking at the outcome of the averaging process as in Fig. 11b): The deformation θ for the averaged distorted Penrose tiling tends to be piecewise (almost) constant in a lot of regions. But then, the distribution of the edge lengths cannot be smooth.

One also observes that in the averaged case there are 1-2-edges and 3-4-edges which have length less than 1, but less 2-3-edges which have length bigger than 1. These are mainly due to vertices of regions no. 1 and 5 (cf.

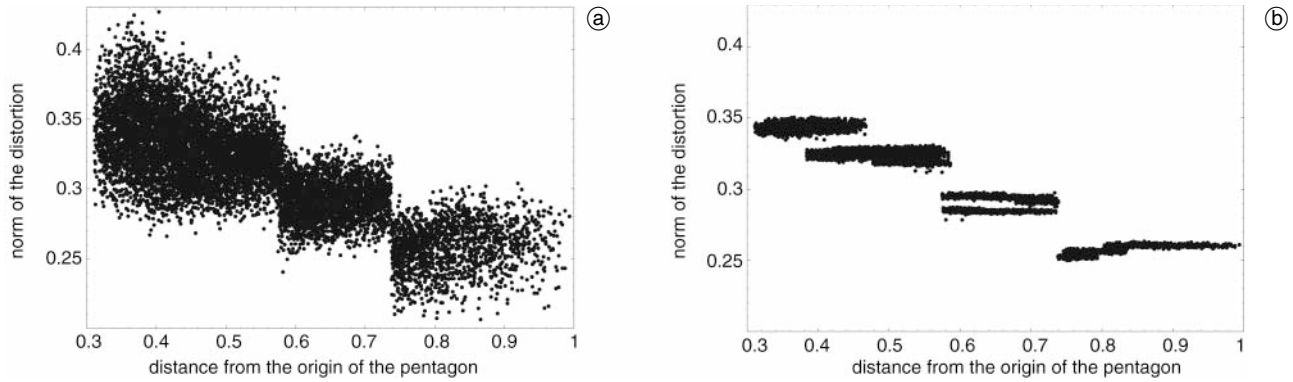

Fig. 11. The norm of the distortions in region no. 2 of Fig. 4 for (**a**) the distorted Penrose tiling and (**b**) the averaged distorted Penrose tiling.

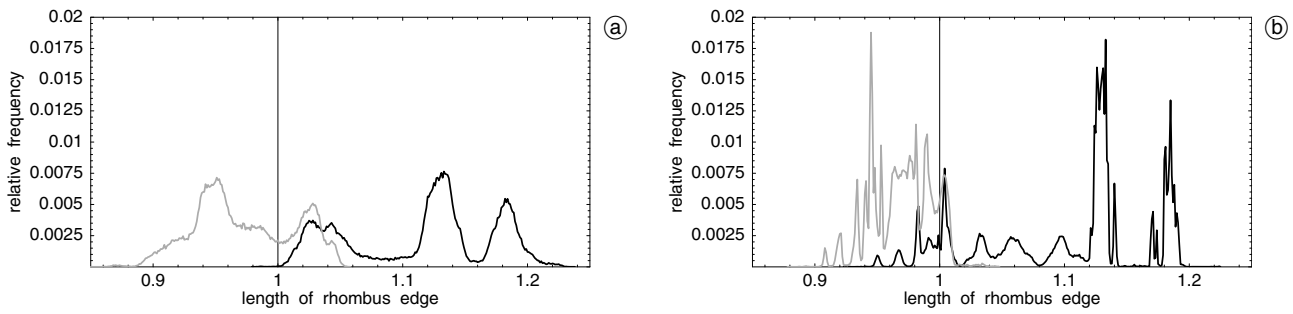

Fig. 12. The (relative) frequency with which different rhombus edge lengths occur in (**a**) a distorted Penrose tiling and (**b**) the averaged distorted Penrose tiling. The distribution of 1-vertex-2-vertex edges and of 3-vertex-4-vertex edges is combined and plotted in black, the distribution of 2-vertex-3-vertex edges is plotted in gray.

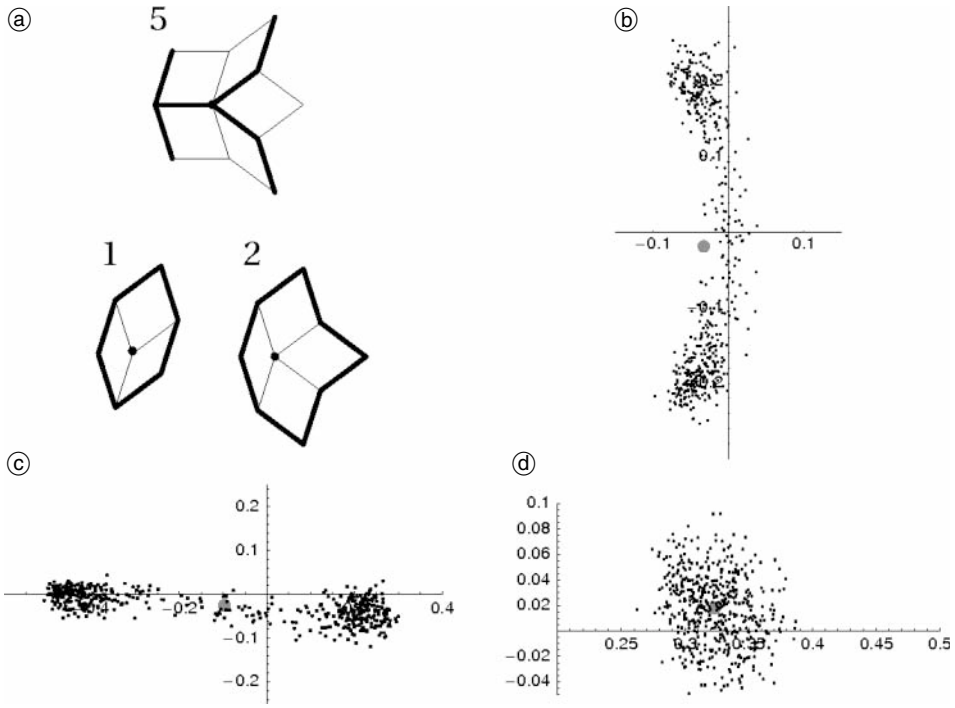

Fig. 13 (**a**) The neighbourhood of the vertices from region no. 1, 2 and 5 (cf. Fig. 4) as in Fig. 5, but here the contracting 2-3-edges are indicate by a bold line. The final distortions of a vertex from (**b**) region 5, (**c**) region 1 and (**d**) region 2 in the 500 simulated distorted Penrose tilings. The averaging procedure yields the gray position in each case (mean of the 500 black points).

Fig. 4) where averaging has the most dramatic effect, compare Fig. 8a) to Fig. 8b) and Fig. 9a) to Fig. 9b). But we also note that some peaks are present in both distributions, namely around 0.95, 1.13 and 1.19, only they are smoothed out for the distorted Penrose tiling. In order to see where in the tiling these differently expanded and contracted edges occur we refer to Figs. 7a) and 7b).

We finally take a closer look at a vertex of regions no. 1, 5 and 2 (cf. Fig. 4). This enables us to put some of the claims above about the behaviour of vertices from regions no. 1 and 5 on a more solid ground. In all three cases the neighbourhood is axis symmetrical, see Fig. 13a). But by the combination of contracting and expanding edges, this symmetry is broken in a distorted Penrose tiling in case of vertices of regions no. 1 and 5, see Figs. 13b) and 13c). There are two clusters of points representing the final distortions on each side of the symmetry axis where such a vertex goes with approximately equal probability. Therefore, such vertices are very sensitive in the MC simulation. We also see why the averaging procedure has such a dramatic effect in these cases: the averaged position lies "somewhere" between the two clusters. For comparison, we have also given an example of a "well-behaved" vertex of region no. 2, see Fig. 13d).

3.8 An MPEG file

A copy of an MPEG video file may be obtained from the authors upon request on a DVD. On this video, we have varied the parameter ε between -0.15 and 0.15, therefore one can also study distorted Penrose tilings at parameters different from $\varepsilon = +.15$. A single screen in this video consists of several regions, so one can see (for the actual parameter ε) the counterparts of Figs. 7a), 8a), 8c), 9a), 9c), 10a) and 12a) in one screen.

4. Discussion

We have carefully explained the concept of a deformed model set in this article. We also put this concept in relation to well-known phenomena like the Debye-Waller effect. Contrary to effects which arise because of some disorder phenomena, a deformed model set is obtained from a (ideal) model set in a deterministic way: There is a continuous function (from the internal to the direct space), the deformation, which describes how each atom is displaced. Although in direct space such a deformation might look at first sight like some kind of disorder phenomenon, there is persistence of pure point diffraction, *i.e.*, no diffuse scattering arises because of such a deformation.

It was observed in [41, 15] that size-effect-like distortions in quasicrystals yield an intensity transfer not (only) on the diffuse scattering – as in crystals – but (mainly) on the pure point part, *i.e.*, the Bragg peaks. In this article we used the toy model of [41] to show that (and to what extent) distorted Penrose tiling can be understood in terms of deformed model sets. Therefore, we were able to explain the observed intensity transfer. This example was chosen to demonstrate that there are additional effects possible in quasicrystals which affect the diffraction pattern, and which have no counterpart in the "crystalline world".

The authors hope that this work helps the reader to gain some insight and is of general use in the structure determination of quasicrystals. We also hope that it initiates some further work in both communities, experimentalists and theoreticians.

Acknowledgments BS acknowledges financial support by the Cusanuswerk and the German Research Council, Collaborative Research Centre 701. BS also thanks Michael Baake for valuable discussions, the RSC at the ANU and the Cusanuswerk for financing a profitable stay and trip to Canberra. TRW would like to acknowledge the support of the Australian Research Council and the Australian Partnership for Advanced Computing.

References

[1] Baake, M.; Höffe, M.: Diffraction of random tilings: Some rigorous results. J. Stat. Phys. **99** (2000) 219–261; http://arxiv.org/abs/math-ph/9901008.

[2] Baake, M.; Kramer, P.; Schlottmann, M.; Zeidler, D.: Planar patterns with fivefold symmetry as sections of periodic structures in 4-space. Int. J. Mod. Phys. B**4** (1990) 2217–2268.

[3] Baake, M.; Lenz, D.: Deformation of Delone dynamical systems and pure point spectrum. J. Fourier Anal. Appl. **11** (2005) 125–150; http://arxiv.org/abs/math.MG/0404155.

[4] Baake, M.; Moody, R. V.: Multi-component model sets and invariant densities. In: *Aperiodic '97* (Eds. M. de Boissieu, J.-L. Verger-Gaugry, R. Currat), pp. 9–20. World Scientific 1998; http://arxiv.org/abs/math-ph/9809005.

[5] Baake, M.; Moody, R. V.: Diffractive point sets with entropy. J. Phys. A: Math. Gen. **31** (1998) 9023–9039; http://arxiv.org/abs/math-ph/9809002.

[6] Baake, M.; Moody, R. V.: Weighted Dirac combs with pure point diffraction. J. reine angew. Math. **573** (2004) 61–94; http://arxiv.org/abs/math.MG/0203030.

[7] Baake, M.; Moody, R. V.: Pure point diffraction. J. Non-Cryst. Solids **334–335** (2004) 77–82.

[8] Baake, M.; Moody, R. V.; Richard, C.; Sing, B.: Which distributions of matter diffract? – Some answers. In: *Quasicrystals: Structure and Physical Properties* (Ed. H.-R. Trebin), pp. 188–207. Wiley-VCH, Berlin 2003; http://arxiv.org/abs/math-ph/0301019.

[9] Baake, M.; Schlottmann, M.; Jarvis, P. D.: Quasiperiodic tilings with tenfold symmetry and equivalence with respect to local derivability. J. Phys. A: Math. Gen. **24** (1991) 4637–4654.

[10] Baake, M.; Sing, B.: Kolakoski$(3,1)$ is a (deformed) model set. Canad. Math. Bull. **47** (2004) 168–190; http://arxiv.org/abs/math.MG/0206098.

[11] Baake, M.; Sing, B.: Diffraction spectrum of lattice gas models above T_c. Lett. Math. Phys. **68** (2004) 165–173; http://arxiv.org/abs/math-ph/0405064.

[12] Bernuau, G.; Duneau, M.: Fourier analysis of deformed model sets. In: *Directions in Mathematical Quasicrystals* (Eds. M. Baake, R. V. Moody), pp. 43–60. CRM Monograph Series vol. **13**, AMS, Providence, RI, 2000.

[13] Butler, B. D.; Withers, R. L.; Welberry, T. R.: Diffuse absences due to the atomic size effect. Acta Cryst. A**48** (1992) 737–746.

[14] Butler, B. D.; Welberry, T. R.: Analysis of diffuse scattering from the mineral mullite. J. Appl. Cryst. **27** (1994) 742–754.

[15] Estermann, M. A.; Lemster, K.; Haibach, T.; Steurer, W.: Towards the real structure of quasicrystals and approximants by analysing diffuse scattering and deconvolving the Patterson. Z. Kristallogr. **215** (2000) 584–596.

[16] Gähler, F.: personal communication.

[17] Henley, C. L.: Random tiling models. In: *Quasicrystals: The State of the Art* (Eds. D. P. DiVincenzo and P. J. Steinhardt), pp. 459–560. 2nd ed., World Scientific, Singapore 1999.

[18] Herbstein, F. H.; Borie Jr., B. S.; Averbach, B. L.: Local atomic displacements in solid solutions. Acta Cryst. **9** (1956) 466–471.

[19] Hof, A.: Diffraction by aperiodic structures at high temperatures. J. Phys. A: Math. Gen. **28** (1995) 57–62.

[20] Hof, A.: Diffraction by aperiodic structures. In: *The Mathematics of Long-Range Aperiodic Order* (Ed. R. V. Moody), pp. 239–268. NATO ASI Series C **489**, Kluwer, Dordrecht 1997.

[21] Höffe, M.: Diffraktionstheorie stochastischer Parkettierungen, PhD-Thesis, Shaker, Aachen (2001).

[22] Ishimasa, T.; Nissen, H.; Fukano, Y.: New ordered state between crystalline and amorphous in Ni–Cr particles. Phys. Rev. Lett. **55** (1985) 511–513.

[23] Ishihara, K. N.; Yamamoto, A.: Penrose patterns and related structures. I. Superstructure and generalized Penrose patterns. Acta Cryst. A**44** (1988) 508–516.

[24] Kramer, P.; Neri, R.: On periodic and non-periodic spacefillings of $\mathbb{E}^m$ obtained by projection. Acta Cryst. A**40** (1984) 580–587. Kramer, P.; Neri, R.: On periodic and non-periodic spacefillings of $\mathbb{E}^m$ obtained by projection. Erratum. Acta Cryst. A**41** (1985) 619.

[25] Kreisel, J.; Bouvier, P.; Dkhil, B.; Thomas, P. A.; Glazer, A. M.; Welberry, T. R.; Chaabane, B.; Mezouar, M.: High-pressure *X*-ray scattering of oxides with nanoscale local structure: Application to $Na_{1/2}Bi_{1/2}TiO_3$. Phys. Rev. B**68** (2003) 014113 (7 pages).

[26] Külske, C.: Universal bounds on the selfaveraging of random diffraction measures. Probab. Theory Relat. Fields **126** (2003) 29–50; http://arxiv.org/abs/math-ph/0109005.

[27] Mermin, N. D.: (Quasi)Crystallography is better in Fourier space. In: *Quasicrystals: The State of the Art* (Eds. D. P. DiVincenzo and P. J. Steinhardt), pp. 137–195. 2nd ed., World Scientific, Singapore 1999.

[28] Moody, R. V.: Model sets: A survey. In: *From Quasicrystals to More Complex Systems* (Eds. F. Axel, F. Dénoyer, J. P. Gazeau), pp. 145–166. EDP Sciences, Les Ulis and Springer, Berlin 2000; http://arxiv.org/abs/math.MG/0002020.

[29] Proffen, T.; Neder, R. B.: DISCUS, a program for diffuse scattering and defect structure simulation. J. Appl. Cryst. **30** (1997) 171–175.

[30] Schlottmann, M.: Generalized model sets and dynamical systems. In: *Directions in Mathematical Quasicrystals* (Eds. M. Baake, R. V. Moody), pp. 143–159. CRM Monograph Series vol. **13**, AMS, Providence, RI, 2000.

[31] Senechal, M.: Quasicrystals and Geometry. Cambridge Univ. Press, Cambridge (1995).

[32] Shechtman, D.; Blech, I.; Gratias, D.; Cahn, J.: Metallic phase with long-range orientational order and no translational symmetry. Phys. Rev. Lett. **53** (1984) 1951–1953.

[33] Sing, B.: Kolakoski sequences – an example of aperiodic order. J. Non-Cryst. Solids **334–335** (2004) 100–104.

[34] Steurer, W.: Twenty years of structure research on quasicrystals. Part 1. Pentagonal, octagonal, decagonal and dodecagonal quasicrystals. Z. Kristallogr. **219** (2004) 391-446.

[35] Warren, B. E.; Averbach, B. L.; Roberts, B. W.: Atomic size effect in the X-ray scattering by alloys. J. Appl. Phys. **22** (1951) 1493–1496.

[36] Welberry, T. R.: Multi-site correlations and the atomic size effect. J. Appl. Cryst. **19** (1986) 382–389.

[37] Welberry, T. R.; Butler, B. D.: Interpretation of diffuse X-ray scattering via models of disorder. J. Appl. Cryst. **27** (1994) 205–231.

[38] Welberry, T. R.; Butler, B. D.; Thompson, J. G.; Withers, R. L.: A 3D model for the diffuse scattering in cubic stabilized zirconias. J. Solid State Chem. **106** (1993) 461–475.

[39] Welberry, T. R.; Christy, A. G.: Defect distribution and the diffuse *X*-ray diffraction pattern of wüstite, $Fe_{1-x}O$. Phys. Chem. Minerals **24** (1997) 24–38.

[40] Welberry, T. R.; Glazer, A. M.: Diffuse *X*-ray scattering in potasssium lithium sulfate, $KLiSO_4$. J. Appl. Cryst. **27** (1994) 733–741.

[41] Welberry, T. R.; Honal, M.: 'Size-effect'-like distortions in quasicrystalline structures. Z. Kristallogr. **217** (2002) 422–426.

[42] Welberry, T. R.; Mayo, S. C.: Diffuse *X*-ray scattering and Monte-Carlo study of guest-host interaction in urea inclusion compounds. J. Appl. Cryst. **29** (1996) 353–364.

[43] Yamamoto, A.; Ishihara, K. N.: Penrose patterns and related structures. II. Decagonal quasicrystals. Acta Cryst. A**44** (1988) 707–714.